A dual scale volume-of-fluid approach for modeling turbulent phase interface dynamics

By M. Herrmann†

In this report, a dual-scale modeling approach is presented to describe turbulent two-phase interface dynamics in a Large Eddy Simulation spatial filtering context. To close the unclosed terms related to the phase interface arising from filtering the Navier-Stokes equation, a resolved realization of the phase interface is explicitly filtered. This resolved realization is maintained on a high resolution over-set mesh using a Refined Local Surface Grid approach employing an un-split, geometric, bounded, and conservative Volume of Fluid method. While the required model for the resolved realization of the interface advection velocity includes the effects of sub-filter surface tension, sub-filter shear, and turbulent eddies, the focus in this report will be on advection by sub-filter turbulent eddies. Examples of a two-dimensional Rayleigh-Taylor instability and the motion of an interface in homogeneous isotropic turbulence are presented.

1. Introduction

Atomization of liquids is a key component in many natural phenomena and technical processes. The atomization of a turbulent petroleum jet issuing from a deep water leak, for example, dictates the drop size distribution of the rising petroleum and determines whether oil will be trapped in the halocline/thermocline of the ocean or rise to the ocean surface to form an oil slick.

Atomization in turbulent environments involves a vast range of length and time scales. Predictive simulations aiming to resolve all relevant scales thus require enormous computational resources, taxing even the most powerful computers available today (Gorokhovski & Herrmann 2008). Since primary atomization is governed by the dynamics of the interface, a need therefore exists for appropriate interface dynamics models that make the computational cost of predicting the atomization outcome more tractable.

A wide range of phenomenological models aiming to represent statistically the essential features of atomization have been proposed in the past. Although these aim to introduce the dominant mechanisms for breakup, they use round blobs injected from the nozzle exit and hence neglect all details of the interface dynamics.

Other modeling approaches to atomization include stochastic models (Gorokhovski *et al.* 2006, 2007) representing the interface by constituent stochastic particles and the mean interface density transport equation model for Reynolds-Averaged Navier-Stokes (RANS) approaches (Vallet & Borghi 1998; Vallet *et al.* 2001). The former treats the interface dynamics in a stochastic sense but requires the *a priori* knowledge of the breakup mechanism, the latter is affected by the drawbacks of the RANS approach: the transport of the mean interface density is modeled by a diffusion-like hypothesis, thereby neglecting the spatial grouping effects of liquid elements (Gorokhovski & Herrmann 2008).

In the context of Large Eddy Simulations (LES), Labourasse *et al.* (2007); Toutant

† School for Engineering of Matter, Transport and Energy, Arizona State University

et al. (2008, 2009*b*,*a*) have proposed models to close the unclosed terms arising from the introduction of spatial filtering into the governing equations. However these models typically neglect the contribution of the sub-filter surface tension term and are based on a cascade process hypothesis that may be questionable in the context of surface tension driven atomization.

In Herrmann (2013); Herrmann & Gorokhovski (2009) a dual-scale modeling approach for LES of interface dynamics was introduced when sub-filter surface tension forces are dominant. This is the case during the final stages of topology change events, where length scales approach zero, or for immiscible fluids of similar densities and viscosities, like petroleum jets in water. The approach is based on the Refined Level Set Grid method (Herrmann 2008) using a level set approach to capture the location of the phase interface.

The purpose of this report is to extend this dual-scale modeling approach to volume-of-fluid interface capturing, creating a Refined Local Surface Grid (RLSG) approach, and to expand the model to include the effects of sub-filter turbulent velocity fluctuations.

2. Governing equations

The equations governing the fully-resolved motion of an unsteady, incompressible, immiscible, two-fluid system are the Navier-Stokes equations,

$$\frac{\partial \rho \boldsymbol{u}}{\partial t} + \nabla \cdot (\rho \boldsymbol{u} \otimes \boldsymbol{u}) = -\nabla p + \nabla \cdot \left(\mu \left(\nabla \boldsymbol{u} + \nabla^T \boldsymbol{u}\right)\right) + \boldsymbol{T}_\sigma \,, \tag{2.1}$$

where $\boldsymbol{u}$ is the velocity, ρ the density, p the pressure, μ the dynamic viscosity, and $\boldsymbol{T}_\sigma$ the surface tension force which is non-zero only at the location of the immiscible interface $\boldsymbol{x}_f$. Furthermore, the continuity equation results in a divergence-free constraint on the velocity field,

$$\nabla \cdot \boldsymbol{u} = 0 \,. \tag{2.2}$$

Assuming ρ and μ are constant within each fluid, density and viscosity can be calculated from

$$\rho = \psi \rho_l + (1-\psi)\rho_g \tag{2.3}$$

$$\mu = \psi \mu_l + (1-\psi)\mu_g \,, \tag{2.4}$$

where indices l and g denote values in liquid and gas, respectively, and ψ is a volume-of-fluid scalar that is $\psi = 0$ in the gas and $\psi = 1$ in the liquid with

$$\frac{\partial \psi}{\partial t} = -\boldsymbol{u} \cdot \nabla \psi = -\nabla \cdot (\boldsymbol{u}\psi) + \psi \nabla \cdot \boldsymbol{u} \,. \tag{2.5}$$

Here, the last term on the right-hand-side is zero for incompressible flows, see Eq. (2.2).

The interface normal vector $\boldsymbol{n}$ and the interface curvature κ can theoretically be expressed in terms of the volume-of-fluid scalar as

$$\boldsymbol{n} = \frac{\nabla \psi}{|\nabla \psi|} \,, \quad \kappa = \nabla \cdot \boldsymbol{n} \,. \tag{2.6}$$

Following the continuum surface force approach by Brackbill *et al.* (1992), the surface tension force $\boldsymbol{T}_\sigma$ in Eq. (2.1) is

$$\boldsymbol{T}_\sigma(\boldsymbol{x}) = \sigma \kappa \delta(\boldsymbol{x} - \boldsymbol{x}_f)\boldsymbol{n} = \sigma \kappa \nabla \psi \,, \tag{2.7}$$

with σ the constant surface tension coefficient and δ the Dirac delta function.

2.1. *Filtered governing equations*

Introducing spatial filtering into Eqs. (2.1) and (2.2) and assuming that the filter commutes with both the time and spatial derivatives, the filtered governing equations can be derived (Toutant *et al.* 2008),

$$\frac{\partial \overline{\rho}\,\overline{\boldsymbol{u}}}{\partial t} + \nabla\cdot(\overline{\rho}\bar{\boldsymbol{u}}\otimes\overline{\boldsymbol{u}}) = -\nabla\bar{p} + \nabla\cdot(\overline{\mu}(\nabla\overline{\boldsymbol{u}} + \nabla^T\overline{\boldsymbol{u}})) + \overline{\boldsymbol{T}}_\sigma + \boldsymbol{\tau}_1 + \nabla\cdot(\boldsymbol{\tau}_2+\boldsymbol{\tau}_3)\,, \tag{2.8}$$

$$\nabla\cdot\bar{\boldsymbol{u}} = 0\,, \tag{2.9}$$

where $\bar{}$ indicates spatial filtering, and

$$\overline{\boldsymbol{T}}_\sigma = \overline{\sigma\kappa\delta(\boldsymbol{x}-\boldsymbol{x}_f)\boldsymbol{n}} \tag{2.10}$$

$$\boldsymbol{\tau}_1 = \frac{\partial\overline{\rho}\,\overline{\boldsymbol{u}}}{\partial t} - \frac{\partial\overline{\rho\boldsymbol{u}}}{\partial t} \tag{2.11}$$

$$\boldsymbol{\tau}_2 = \overline{\rho}\,\overline{\boldsymbol{u}}\otimes\overline{\boldsymbol{u}} - \overline{\rho\boldsymbol{u}\otimes\boldsymbol{u}} \tag{2.12}$$

$$\boldsymbol{\tau}_3 = \overline{\mu(\nabla\boldsymbol{u}+\nabla^T\boldsymbol{u})} - \overline{\mu}(\nabla\overline{\boldsymbol{u}}+\nabla^T\overline{\boldsymbol{u}})\,, \tag{2.13}$$

where $\overline{\boldsymbol{T}}_\sigma$ is the filtered surface tension force, and $\boldsymbol{\tau}_1$, $\boldsymbol{\tau}_2$, and $\boldsymbol{\tau}_3$ are associated respectively with acceleration, advection, and viscous effects (Toutant *et al.* 2008). Using Eqs. (2.3) and (2.4), the filtered density and viscosity in Eq. (2.8) are

$$\overline{\rho} = \rho_l\overline{\psi} + \rho_g(1-\overline{\psi}) \tag{2.14}$$

$$\overline{\mu} = \mu_l\overline{\psi} + \mu_g(1-\overline{\psi})\,, \tag{2.15}$$

where

$$\overline{\psi} = \int \mathcal{G}(\boldsymbol{x})\psi d\boldsymbol{x}\,, \tag{2.16}$$

and $\mathcal{G}$ is a normalized spatial filter function.

For the case where sub-filter surface tension contributions are negligible, Toutant *et al.* (2008) proposed models for $\boldsymbol{\tau}_1$, $\boldsymbol{\tau}_2$, and $\boldsymbol{\tau}_3$. For the case where sub-filter surface tension contributions are dominant, Herrmann (2013) proposed a dual-scale modeling approach that neglected the contributions of $\boldsymbol{\tau}_1$, $\boldsymbol{\tau}_2$, and $\boldsymbol{\tau}_3$, thus being applicable to flows with small viscosity and density contrasts, for example water/oil systems, and scenarios with small sub-filter turbulent transport.

In this report, we extend this dual-scale modeling approach for small viscosity and density contrast flows, to flows with non-negligible sub-filter turbulent transport of both momentum and the phase interface, focusing solely on the terms associated with these effects. We thus neglect $\boldsymbol{\tau}_1$, $\boldsymbol{\tau}_2$, and $\overline{\boldsymbol{T}}_\sigma$. For $\boldsymbol{\tau}_3$, we employ a standard dynamic Smagorinsky modeling approach, leaving $\overline{\psi}$ as the quantity that requires modeling.

3. The dual-scale approach to modeling sub-filter interface dynamics

Instead of relying on a cascade process by which dynamics on a sub-filter scale can be inferred from the dynamics on the resolved scale, the dual-scale approach proposed in Herrmann & Gorokhovski (2009) aims to maintain a fully resolved realization of the immiscible interface geometry at all times, expressed, for example, in terms of a volume-of-fluids scalar ψ. Then $\overline{\psi}$ can be calculated exactly by explicit filtering using Eq. (2.16).

Although this is an exact closure, the problem of modeling is of course simply shifted to the problem of maintaining a fully resolved realization of the interface geometry, i.e., describing the fully resolved motion of the interface, Eq. (2.5). Since the fully resolved

velocity is the sum of the filtered velocity and the sub-grid velocity, $\boldsymbol{u} = \overline{\boldsymbol{u}} + \boldsymbol{u}_{sg}$, this results in the

$$\frac{\partial \psi}{\partial t} = -\nabla \cdot \left(\left(\overline{\boldsymbol{u}} + \boldsymbol{u}_{sg} \right) \psi \right) + \psi \nabla \cdot \left(\overline{\boldsymbol{u}} + \boldsymbol{u}_{sg} \right) \tag{3.1}$$

where the only term requiring modeling is $\boldsymbol{u}_{sg}$.

In Herrmann & Gorokhovski (2009) a model for $\boldsymbol{u}_{sg}$ is proposed consisting of three contributions,

$$\boldsymbol{u}_{sg} = \boldsymbol{u}' + \delta \boldsymbol{u} + \boldsymbol{u}_{\sigma} \, , \tag{3.2}$$

where $\boldsymbol{u}'$ is due to sub-filter turbulent eddies, $\delta \boldsymbol{u}$ is attributed to the interface velocity increment due to relative sub-filter motion between the two immiscible fluids, and $\boldsymbol{u}_{\sigma}$ is due to sub-filter velocities induced by sub-filter surface tension forces. The focus of the current report is on the first term; for a modeling outline of the second term, the reader is referred to Herrmann & Gorokhovski (2009, 2008), and for modeling of the last term, the reader is referred to Herrmann (2013).

3.1. *The resolved interface velocity due to filtered transport and sub-filter eddies*

The fully resolved interface realization is advected by $\boldsymbol{u} = \overline{\boldsymbol{u}} + \boldsymbol{u}'$. Here $\overline{\boldsymbol{u}}$ is simply the solution of the filtered Navier-Stokes equation, Eq. (2.8), and $\boldsymbol{u}'$ is the velocity of sub-filter turbulent eddies that requires modeling. Different modeling strategies for $\boldsymbol{u}'$ can be devised, including deconvolution approaches, however, in this report, as a first feasibility test, we will use a velocity database obtained from direct numerical simulation of homogeneous isotropic turbulence (McCaslin & Desjardins 2014).

4. Numerical methods

To efficiently solve Eq. (3.1) for the fully resolved immiscible interface, the RLSG method (Herrmann 2008) is used. By design, it solves the interface capturing advection equation on a separate, highly resolved Cartesian overset grid of mesh spacing h_G, independent of the underlying flow solver grid of mesh spacing h, using a dual narrow-band approach. The numerical approach is optimized for massively parallel computer systems and allows for significantly refined overset-grids at low cost compared to the flow solver cost (Herrmann 2008).

However, instead of employing a level set approach to capture the interface as in Herrmann (2008, 2013), here, we will use a volume-of-fluid approach. The advantage over the level set approach is that the volume-of-fluid approach can be constructed to be inherently mass conserving, i.e., the volume of each fluid is conserved individually. We use the recently proposed unsplit geometric transport scheme for volume-of-fluid scalars by Owkes & Desjardins (2014) that ensures both discrete volume conservation of each fluid and boundedness of the volume-of-fluid scalar ψ. Geometric reconstruction of the interface within each computational cell is done using PLIC reconstruction, employing the analytical formulas of Scardovelli & Zaleski (2000) using ELVIRA estimated normals (Pilliod 1992; Pilliod Jr. & Puckett 2004).

The unsplit, geometric advection scheme of Owkes & Desjardins (2014) requires face-centered velocities that are discretely divergence-free to ensure both conservation and boundedness. While discretely divergence-free filtered velocities $\overline{\boldsymbol{u}}$ are available on the flow solver mesh due to the application of a projection step of the velocities in a standard fractional step method, such velocities $\boldsymbol{u}$ are not directly available on the fine overset mesh. Since $\boldsymbol{u} = \overline{\boldsymbol{u}} + \boldsymbol{u}_{sg}$, both $\overline{\boldsymbol{u}}$ and $\boldsymbol{u}_{sg}$ need to be discretely divergence free on the fine

overset mesh. To ensure $\nabla_{h_G} \cdot \overline{\boldsymbol{u}} = 0$ if $\nabla_h \cdot \overline{\boldsymbol{u}} = 0$, we employ the optimal constrained approach for divergence-free velocity interpolation by Cervone *et al.* (2011), recursively applying the interpolation technique for nested staggered meshes up to the refinement level of the overset mesh. Note that the choice of this interpolation technique limits the type of fine resolution overset meshes for the fully resolved interface realization to staggered meshes, nested within the flow solver mesh, i.e. $h_G = h/2^p$. For non-nested meshes and/or non-divergence preserving interpolation techniques, an additional projection step on the fine overset mesh would be required to ensure that the interpolated velocities are discretely divergence free.

In this study, $\boldsymbol{u}_{sg} = \boldsymbol{u'}$ with $\boldsymbol{u'}$ determined from direct numerical simulation (DNS) of homogeneous isotropic turbulence (McCaslin & Desjardins 2014). To calculate $\boldsymbol{u'}$, the DNS velocity field $\boldsymbol{u}^{DNS}$ is first filtered using a top-hat filter to the desired LES mesh spacing h, yielding $\overline{\boldsymbol{u}}^h$. The sub-filter fluctuation velocity on the DNS mesh is then $\boldsymbol{u'}^{DNS} = \boldsymbol{u}^{DNS} - \overline{\boldsymbol{u}}^h$. This sub-filter fluctuation velocity is then filtered to the desired overset mesh resolution h_G yielding $\boldsymbol{u'}^{h_G}$ and projected into the subspace of divergence free velocities to ensure the velocities are discretely divergence free.

Finally, to calculate $\overline{\psi}$, Eq. (2.16) is evaluated by setting the filter size to the local flow solver mesh spacing h and evaluating the integral by explicitly summing VoF scalar ψ of those overset-mesh cells that are contained within a given flow solver cell.

5. Results

Results for two test cases are given in this section. First, to test the recursively divergence-free preservation of the velocity interpolation scheme and to analyze the performance of the volume-of-fluid overset mesh method, a two-dimensional Rayleigh-Taylor test case is presented. Second, the results of the dual-scale approach for the deformation of a unit density and viscosity ratio interface in homogeneous isotropic turbulence are discussed (McCaslin & Desjardins 2014).

5.1. *Rayleigh-Taylor instability*

A heavy fluid, $\rho_1 = 1.225$, $\mu_1 = 0.00313$, is placed above a light fluid, $\rho_2 = 0.1694$, $\mu_2 = 0.00313$, inside a domain of size 1x4. The interface between the two fluids is placed in the middle of the domain and is perturbed by a cosine wave of amplitude 0.05. The gravity constant is set to $g = 9.81$ and no turbulent sub-grid velocities are imposed, $\boldsymbol{u'} = 0$. We set the time step size constant to $\Delta t = 1.25 \cdot 10^{-4}$ and simulate up to $t = 0.9$. Using a Cartesian flow solver grid of $h = 1/512$ and matching overset-grid of $h_G = 1/512$ results in a solution that is indistinguishable from the reference solution to this case presented for example in Herrmann (2008) and will thus be used as the reference in the following.

Figure 1 shows the interface shape at $t = 0.9$ for different resolutions of the flow solver grid and the overset grid. In the caption, the first number in parentheses is the number of mesh points of the flow solver per unit length, whereas the second number is the number of overset mesh points per unit length. As shown, using 64 points per unit length for both the flow solver and the overset mesh (left most figure) is insufficient to resolve the flow dynamics of the problem and the thin ligament forming. Refining the overset mesh to 256 points per unit length (third figure from the left) provides sufficient resolution to prevent the unphysical breakup of the thin ligament, yet the flow solver resolution is inadequate to give the correct position of the ligament and the end drop. At 128 flow solver mesh points per unit length (center three figures), the interface shape approaches that of the reference solution, however, at 128 overset mesh points per unit length (fourth

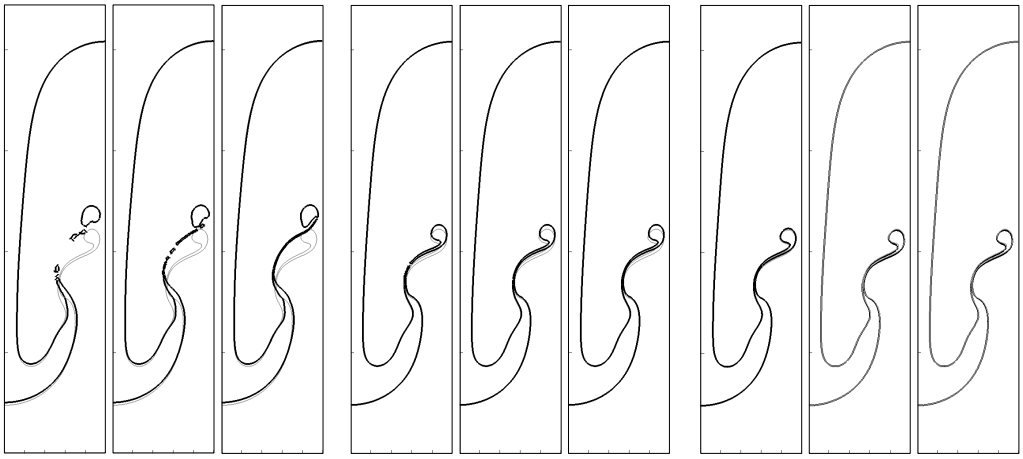

FIGURE 1. Rayleigh-Taylor instability interface shapes at $t = 0.9$ for flow solver mesh (first number) and overset mesh (second number) of (64,64), (64,128), (64,256); (128,128), (128,256), (128,512); (256,256), (256,512), (256,1024), left to right. Thin gray line denotes reference solution.

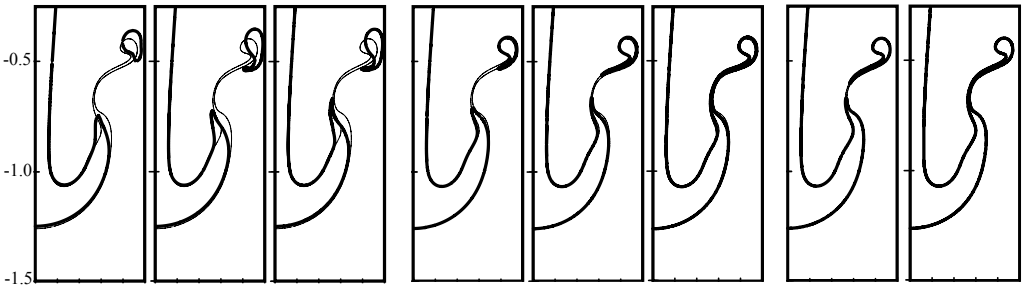

FIGURE 2. Rayleigh-Taylor instability interface shapes at $t = 0.9$ for level set solution on flow solver mesh (first number) and overset mesh (second number) of (64,64), (64,128), (64,256); (128,128), (128,256), (128,512); (256,256), (256,512), left to right (Herrmann 2008). Thin line denotes reference solution.

figure from the left), the thin ligament is again not supported by the overset mesh and breakup occurs. Finally, using 256 fluid solver mesh points per unit length (right three figures), all overset mesh resolutions ranging from 256 to 1024 points per unit length recover the reference solution well.

In all cases, each fluid volume in the system is conserved with machine precision, and the volume-of-fluid scalar remains bounded between zero and one up to machine precision. This demonstrates that the employed recursive divergence preserving velocity interpolation approach is able to yield divergence-free face velocities on arbitrarily refined nested overset meshes.

To compare the obtained volume-of-fluid results to results obtained with the RLSG method using a 5th-order distance function level set approach, Figure 2 (Herrmann 2008) shows the interface shape at $t = 0.9$ using flow and overset mesh resolutions equal to those of Figure 1. At a flow solver mesh resolution of 64 points per unit length (three left most figures), significant differences to the volume-of-fluid solution can be observed. Even at an overset mesh resolution of 256 points per unit length, the thin ligament cannot be maintained, however, the end drop shape and position for the level set solution is closer

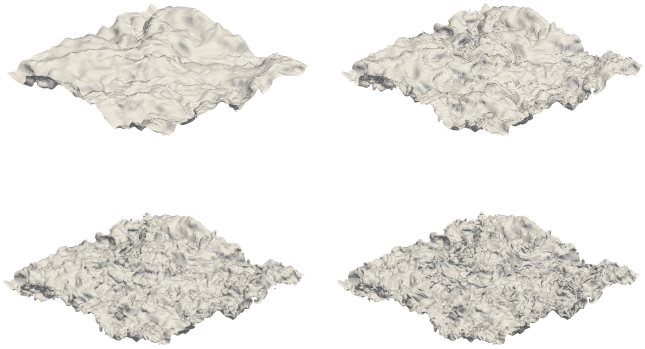

FIGURE 3. PLIC reconstructed interface geometry at $t/t_\lambda = 0.1$ for 32^3 LES mesh with overset mesh of 128^3 without SGS velocity $\boldsymbol{u}'$ (top left), and with SGS velocity $\boldsymbol{u}'$ and overset mesh of 128^3 (top right), 256^3 (bottom left) and 512^3 (bottom right).

to the reference solution than in the volume-of-fluid case (three left most figures of Figure 1). This observation holds true at a flow solver resolution of 128 points per unit length, although a higher resolution of the overset mesh is required to maintain the thin ligament uninterrupted as compared to the volume-of-fluid solution (256 vs 512 mesh points). At a flow solver resolution of 256 mesh points per unit length, both the level set solution and the volume-of-fluid solution are in excellent agreement with the reference solution.

The main difference between the level set and the volume-of-fluid solution lies in the fact that the volume-of-fluid approach used here conserves each fluid volume up to machine precision, whereas the level set approach is susceptible to fluid volume conservation errors that can reach up to 0.3% in the coarsest case (Herrmann 2008). However, as the results show, it is not clear that enforcing discrete fluid volume conservation yields superior results in cases where fluid structures are not supported by the used overset mesh. Indeed, the necessary numerical motion of fluid volume from an unresolvable configuration, i.e. the unsupportable thin ligament in the (64,64) case for example, to a resolvable configuration appears to result in the incorrect additional motion of the end drop upwards. In the level set case, the unsupportable thin ligament simply disappears, violating volume conservation, yet the remaining, supportable end drop maintains a position closer to the reference solution than the volume-of-fluid case.

5.2. *Interface dynamics in homogeneous isoptropic turbulence*

An initially flat interface is placed inside a box of fully developed isotropic turbulence. Both density and viscosity ratio are unity and no surface tension forces are present with a Reynolds number of $\mathrm{Re}_\lambda = 313$ and $\mathrm{We} = \infty$. Direct numerical simulation results using a 1024^3 mesh for this case are reported in McCaslin & Desjardins (2014). Here, we present LES results using the dual scale approach using a LES mesh resolution of 32^3. To study the impact of the sub-filter mesh resolution, the overset mesh resolution is varied from 128^3, 256^3 to 512^3 mesh points, leaving 1024^3 points, the equivalent of the fully resolved case, for future studies. The sub-filter velocity $\boldsymbol{u}'$ is obtained from the DNS field by the procedure outlined in section 3.1 and frozen in time.

Figures 3-5 show the PLIC reconstructed interface geometry after 0.1, 0.2, 0.3, and 0.4 eddy turnover times. The impact of including the sub-filter velocity in the advection

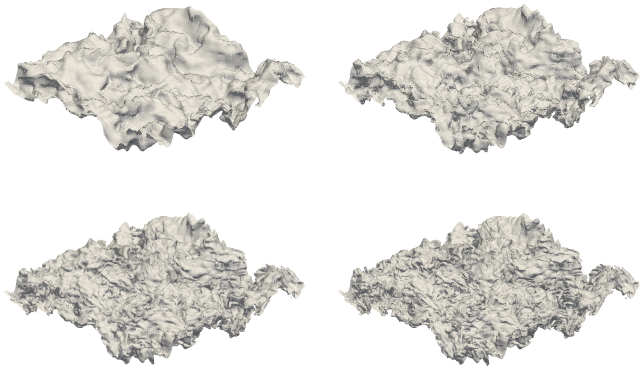

FIGURE 4. PLIC reconstructed interface geometry at $t/t_\lambda = 0.2$ for 32^3 LES mesh with overset mesh of 128^3 without SGS velocity $\boldsymbol{u}'$ (top left), and with SGS velocity $\boldsymbol{u}'$ and overset mesh of 128^3 (top right), 256^3 (bottom left) and 512^3 (bottom right).

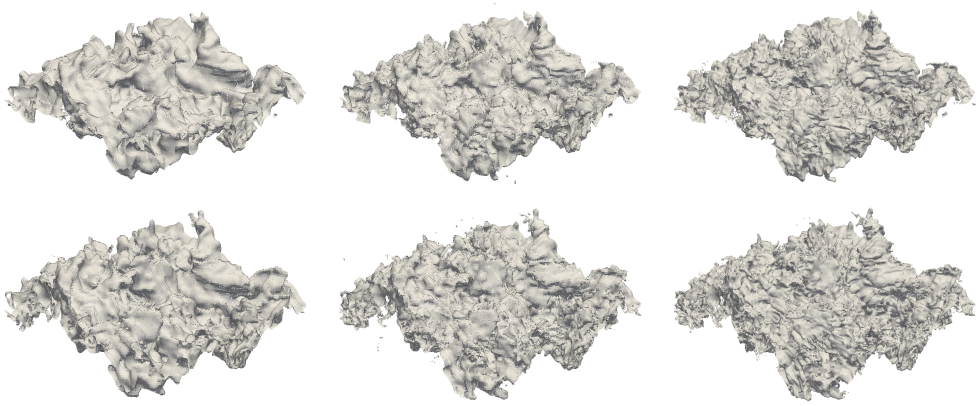

FIGURE 5. PLIC reconstructed interface geometry at $t/t_\lambda = 0.3$ (top row) and 0.4 (bottom row) for 32^3 LES mesh with overset mesh of 128^3 without SGS velocity $\boldsymbol{u}'$ (left), and with SGS velocity $\boldsymbol{u}'$ and overset mesh of 128^3 (middle), 256^3 (right).

velocity of the resolved realization of the interface is clearly noticeable, leading to significantly more surface corrugations with higher overset mesh resolutions, as compared to outright neglecting the contribution. However, limiting the overset mesh resolution to length scales larger than the DNS resolution, as done here, introduces an additional filter in the sub-filter velocity $\boldsymbol{u}'$ resulting in likely fewer surface corrugations as observed in the DNS (McCaslin & Desjardins 2014).

Figure 6 corroborates this observation showing the total interface surface area A as a function of time. Here the surface area is calculated as the total area of the PLIC reconstructed planes in each interface cell. The calculated area is necessarily an underprediction of the true surface area due to the discontinuous nature of the PLIC interface reconstruction across cell faces. As shown, incorporating more scales in the sub-filter velocity $\boldsymbol{u}'$ by increasing the overset mesh resolution increases the total surface area significantly. Processes that depend on the available surface area, for example phase

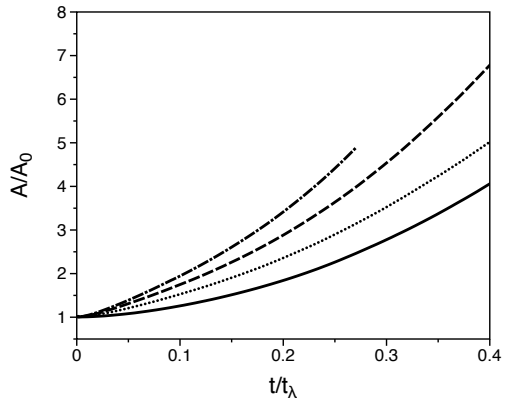

FIGURE 6. Non-dimensional PLIC reconstructed surface area $A/A(t=0)$ as a function of time for LES flow solver mesh of 32^3 mesh points and overset mesh of 128^3 points without SGS velocity $\boldsymbol{u}'$ (solid line), 128^3 with SGS velocity $\boldsymbol{u}'$ (dotted line), 256^3 with SGS velocity $\boldsymbol{u}'$ (dashed line), and 512^3 with SGS velocity $\boldsymbol{u}'$ (dash-dotted line).

change, could thus be strongly impacted by the inclusion of the dual-scale model, as could the atomization behavior in the presence of shear and surface tension forces.

6. Conclusions

A dual scale modeling approach for phase interface dynamics in turbulent flows is presented that is based on a volume-of-fluid approach. The method uses overset high-resolution meshes to capture a resolved realization of the phase interface geometry that can be explicitly filtered to close the terms that require modeling in the filtered Navier-Stokes equations. This report focused solely on the impact of sub-filter velocity fluctuations that, as shown, have a significant impact on the amount of interface surface area generated in turbulent flows. Future work will focus on combining the here-presented sub-filter velocity model to the previously presented dual-scale approach for sub-filter surface tension forces, resulting in a modeling approach that should be applicable to atomization scenarios.

Acknowledgments

The author would like to acknowledge Olivier Desjardins, Vincent Le Chenadec, and Jeremy McCaslin for many helpful discussions during the summer program.

REFERENCES

BRACKBILL, J. U., KOTHE, D. B. & ZEMACH, C. 1992 A continuum method for modeling surface tension. *J. Comput. Phys.* **100**, 335–354.

CERVONE, A., MANSERVISI, S. & SCARDOVELLI, R. 2011 An optimal constrained approach for divergence-free velocity interpolation and multilevel vof method. *Comput. Fluids* **47**, 101–114.

GOROKHOVSKI, M. & HERRMANN, M. 2008 Modeling primary atomization. *Annu. Rev. Fluid Mech.* **40**, 343–366.

GOROKHOVSKI, M., JOUANGUY, J. & CHTAB, A. 2006 Simulation of air-blast atomization: "floating guard" statistic particle method for conditioning of LES computation;

stochastic models of break-up and coalescence. In *International Annual Conference on Liquid Atomization and Spray Systems.*

Gorokhovski, M., Jouanguy, J. & Chtab, A. 2007 Stochastic simulation of the liquid jet break-up in a high-speed air coflow. In *Int. Conf. Multiph. Flow*.

Herrmann, M. 2008 A balanced force refined level set grid method for two-phase flows on unstructured flow solver grids. *J. Comput. Phys.* **227**, 2674–2706.

Herrmann, M. 2013 A sub-grid surface dynamics model for sub-filter surface tension induced interface dynamics. *Comput. Fluids* **87**, 92–101.

Herrmann, M. & Gorokhovski, M. 2008 An outline of a LES subgrid model for liquid/gas phase interface dynamics. *Proceedings of the Summer Program*, Center for Turbulence Research, Stanford University, pp. 171–181.

Herrmann, M. & Gorokhovski, M. 2009 A large eddy simulation subgrid model for turbulent phase interface dynamics. In *ICLASS 2009, 11th Triennial International Annual Conference on Liquid Atomization and Spray Systems*.

Labourasse, E., Lacanette, D., Toutant, A., Lubin, P., Vincent, S., Lebaigue, O., Caltagirone, J. P. & Sagaut, P. 2007 Towards large eddy simulation of isothermal two-phase flows: Governing equations and a priori tests. *Int. J. Multiphase Flow* **33**, 1–39.

McCaslin, J. & Desjardins, O. 2014 Theoretical and computational modeling of turbulence/interface interactions. *Proceedings of the Summer Program*, Center for Turbulence Research, Stanford University.

Owkes, M. & Desjardins, O. 2014 A computational framework for conservative, three-dimensional, unsplit, geometric transport with application to the volume-of-fluid (VOF) method. *J. Comput. Phys.* **270**, 587–612.

Pilliod, J. E. 1992 *An analysis of piecewise linear interface reconstruction algorithms for volume-of-fluid methods.* M.Sc. Thesis, University of California Davis.

Pilliod Jr., J. E. & Puckett, E. G. 2004 Second-order accurate volume-of-fluid algorithms for tracking material interfaces. *J. Comput. Phys.* **199**, 465–502.

Scardovelli, R. & Zaleski, S. 2000 Analytical relations connecting linear interfaces and volume fractions in rectangular grids. *J. Comput. Phys.* **164**, 228–237.

Toutant, A., Chandesris, M., Jamet, D. & Lebaigue, O. 2009*a* Jump conditions for filtered quantities at an under-resolved discontinuous interface. part 1: Theoretical development. *Int. J. Multiphase Flow* **35**, 1100–1118.

Toutant, A., Chandesris, M., Jamet, D. & Lebaigue, O. 2009*b* Jump conditions for filtered quantities at an under-resolved discontinuous interface. part 2: A priori tests. *Int. J. Multiphase Flow* **35**, 1119–1129.

Toutant, A., Labourasse, E., Lebaigue, O. & Simonin, O. 2008 DNS of the interaction between a deformable buoyant bubble and a spatially decaying turbulence: A priori tests for LES two-phase flow modelling. *Comput. Fluids* **37**, 877–886.

Vallet, A. & Borghi, R. 1998 An Eulerian model of atomization of a liquid jet. In *Proc. Int. Conf. Multiph. Flow*. Lyon, France.

Vallet, A., Burluka, A. & Borghi, R. 2001 Development of an Eulerian model for the atomization of a liquid jet. *Atomization Sprays* **11**, 619–642.